arXiv:nucl-th/0404008v1 4 Apr 2004

Relaxation, Emission Modes and Limit Temperatures in Ni+Ni HIC.

Armando Barrañón *; J. A. López †; C. Dorso. ‡

November 15^{th} 2003

Abstract

A dynamical stability analysis is performed for Ni+Ni central collision at intermediate energies, showing that in chemical, thermal and dynamical equilibriums are reached at an early stage of system evolution. This is obtained by computing the relaxation times of the quadrupole momentum, speed of sound and electric charge density of the system. This way, fragment emission modes at low and high energies as well as the qualitative behavior of the limit temperatures are determined.

1 Introduction

In a heavy ions collision, a compound nuclear system is initially formed that will expand as a consequence of the thermal or compressive pressure. Expansion leads the nuclear system into the instability region where the speed of sound attains an imaginary value. At this instability region, system is disassembled into fragments and nucleons. Fragmentation results from an adiabatic expansion of hot nuclear matter produced in the collision that leads the system into the mechanical instability region, where the system fragments into clusters and nucleons due to the increase of density fluctuations [1]. Neutron rich Heavy ions collisions lead to transient states of nuclear matter with high spin asymmetry and with a great thermal and compressive excitation, allowing the exploration of the properties of nuclear matter whose neutron contain goes from pure neutron nuclear matter up to symmetric nuclear matter [2]. Mller et. al. has shown that the liquid-gas phase transition in asymmetric nuclear matter is of second order instead of the first order phase transition observed in symmetric nuclear matter [3].

Several important aspects of nuclear collisions depend on the isospin, such as the nuclear stopping, the collective nuclear flow as well as the balance energy and pre-equilibrium nucleon emission. Bao An-Li et. al. have found that the mean nuclear field domains completely the density fluctuations as well as the isospin fluctuations, meanwhile two-body scattering

*Universidad Autónoma Metropolitana. Unidad Azcapotzalco. Av. San Pablo 124, Col. Reynosa-Tamaulipas, Mexico City. email: bca@correo.azc.uam.mx

†Dept. of Physics, The University of Texas at El Paso. El Paso, TX, 79968

‡Depto.de Física, Universidad de Buenos Aires. Buenos Aires, Argentina

meaningfully influences in the subsequent isospin growth. Both fluctuations are increased in the dynamically instable systems meanwhile in the chemically instable systems only the density fluctuations are increased. The magnitude of both fluctuations diminishes when increases the isospin asymmetry resulting from the decrease of the isoscalar attractive mean field, due to the increase of the neutron symmetric repulsive potential in neutron rich nuclear matter [4]. Beaulieu et. al. analyzed experimental results of heavy ions collisions and found long relaxation times for surface fragment emissions and short relaxation times when fragments are emitted from the bulk [5]. In the soft region of the state equation, the pressure change is much smaller and hence a small speed of sound is attained since it depends directly on the pressure energy gradient: $V^2 = \frac{dP}{de}$.

In this soft region, the collective dynamics of dense and hot matter formed in heavy ion collisions can be determinant. As a matter of fact, a small speed of sound delays the expansion of compressed matter and leads a lighter transverse collective flow [6]. As shown via hydrodynamic models, heavy ion collisions reach the soft region of the state equation when the incident energy varies, building up a fireball that lasts a long time, leading to a minimum in the energy dependence of the collective transverse flow [7].

2 Latino Model.

LATINO model [8] uses semi-classical approximation to simulate intermediate energy heavy ions collisions and replicates binary interaction via Pandharipande potential. This potential is built up with a linear combination of Yukawa potentials, whose coefficients are fitted in order reproduce the properties of nuclear matter. Clusters are recognized using an Early Cluster Recognition Algorithm, that optimizes the configuration in the energy space. Ground states are produced generating a random configuration in phase space, gradually reducing the speed of the particles confined into a parabolic potential, until the theoretical binding energy is reached. Projectile kinetic energy varies in a range going from 800 MeV up to 2000 MeV in the center of mass system, with 200 replicas for each energy. Numerical integration of the equations of motion is performed with a Verlet algorithm with time intervals that ensure energy conservation up to 0.05converge to a power law in this range of intermediate energies [9].

3 Methodology

In the Minimum Spanning Tree in Energy Algorithm (MSTE) , a given set of particles i,j,...,k belongs to the same cluster C_i whenever: $\forall i \in C_i$, there exists $j \in C_i / e_{ij} \leq 0$ where $e_{ij} = V(r_{ij}) + (\mathbf{p}_i - \mathbf{p}_j)^2/4\mu$, and μ is the reduced mass of the pair i,j.

Fragment formation time, t_{ff}, can be defined as the time when the system breaks up in a defined way, namely after t_{ff} fragments evaporate only some monomers. In order to estimate t_{ff} the Microscopic Persistence Coefficient P is used, [10]:

$$P\left[X,Y\right] = \frac{1}{\sum_{cluster} n_i} \sum_{cluster} n_i \frac{a_i}{b_i} \tag{1}$$

where $X \equiv \{C_i\}$ and $Y \equiv \{C'_i\}$ are two partitions, b_i is the number of particle pairs belonging to cluster C_i of partition X, a_i is the number of particle pairs belonging to cluster C_i and also belonging to a given cluster C'_j of partition Y, n_i is the number of particles in cluster C_i .

It is convenient to study the time evolution of the quantities:

$$\hat{P}^{+}\left[X(t)\right] \equiv \left\langle P\left[X(t), X(t \to \infty)\right]\right\rangle_{collisions} \tag{2}$$

$$\hat{P}^{-}\left[X(t)\right] \equiv \left\langle P\left[X(t \to \infty), X(t)\right]\right\rangle_{collisions} \tag{3}$$

$$\hat{P}^{dt}\left[X(t)\right] \equiv \left\langle P\left[X(t), X(t+dt)\right]\right\rangle_{collisions} \tag{4}$$

where $X(t)$ is a partition at time t, $X(t \to \infty)$ is an asymptotic partition, and represents an average on all the collisions. is a partition identical to the partition , except for the fact that a nucleon has been evaporated in each cluster.

$$\lambda = \left.(n/p)\right|_{y>0} / \left.(n/p)\right|_{y\leq 0} \tag{5}$$

where $\left.(n/p)\right|_{y>0}$ and $\left.(n/p)\right|_{y\leq 0}$ are the ratios between the number of neutrons and protons moving forward and backwards, respectively. Dynamical instability is set when the squared speed of sound is negative. Adiabatic speed of sound is given by:

$$V_C^2 = (1/m)\left[(\partial P/\partial\rho)\rangle_S\right] \tag{6}$$

$$V_C^2 = (1/m)\left[(10/9) < E_K > +a(\rho/\rho_0) + b(\rho/\rho_0)^{\sigma}\right] \tag{7}$$

where $< E_K >$ is the mean kinetic energy per nucleon, a=-358.1 MeV, b=304.8 MeV and $\sigma = 7/6$ are the parameters of the soft state equation. When $V_C^2 < 0$ nuclear matter is instable with respect to density fluctuations, leading to dynamical instabilities [11]. Heavy residuals thermal equilibrium can be examined studying the quadrupolar momentum Q_{ZZ} defined by:

$$Q_{ZZ} = \int drdp(2\pi)^3 \left[2p_z^2 - p_y^2 p_x^2\right] f(\overrightarrow{r}, \overrightarrow{p}, t) \tag{8}$$

where $f(\overrightarrow{r}, \overrightarrow{p}, t)$ is Wigner function. Clearly $Q_{ZZ} = 0$ is a necessary but not sufficient condition for thermal equilibrium [12]. Mean Velocity Transfer is given by:

$$MVT_i = \sum_k \left|V_{ki}(t+dt) - V_{ki}(t)\right| \tag{9}$$

4 Relaxation and Instabilities.

Collision Disordered Mode is the only one present in the uniformly excited systems, and is responsible of fragment production as well as the exterior flow dispersing the fragments [13, 14]. MSTE can be used to study biggest fragment size, total multiplicity and persistent coefficients.

Figs. 1a, b and c show time evolution of these three quantities. Due to the initial violent collision, some particles attain lots of energy and are unable to be bound to a fragment even when these particles might be inside or close to a fragment. This reduces the size of the biggest MSTE cluster in this early stage and increases the total multiplicity. Fig, 2 shows

Ni+Ni collision stages for an energy of 1400 MeV. The first stage ends up with a peak of kinetic energy transported by the promptly emitted particles, KE(PEP), signed by the peak of the wide continuous line. The second stage finishes up with the attenuation of the intermediate fragment production (IMF) , shown as a peak in the continuous curve. Between these two peaks, another peak is seen in the intermittent wide curve of the Mean Velocity Transverse (MVT), signing the onset of the instabilities. As can be seen, MVT produce instabilities leading to light particle emission and subsequent intermediate fragment emission (IMF). Once the continuous curve is attenuated, a final stage is installed with slow light fragment emission and system freezing-up. Persistent coefficients P^+ and P^- computed using MSTE partitions, can be sed to understand how the partition attains its microscopic composition at an asymptotic time.

In this study dynamical, thermal and chemical instability signals are used to detect the relaxation times for several projectile energies, that are expected to reach a peak in the second collision stage and attenuate at the third collision stage. Fig. 3 shows the time evolution of the parameter λ with a peak signing the entrance into the chemical instability zone, for the Ni+Ni central collision with a projectile energy of 1400 MeV. When the system attains chemical equilibrium, the parameter λreaches a value close to zero. Fig. 4 shows the time evolution of the normalized quadrupole momentum with a peak signing the entrance into the thermal instability zone, for the central collision Ni+Ni, for a projectile energy of 1400 MeV. When the system attains thermal equilibrium, the normalized quadrupolar momentum reaches a value close to zero. Fig. 5 shows time evolution of the squared adiabatic speed of sound with a peak signing the entrance into the dynamical instability zone, for Ni+Ni central collision with a projectile energy of 1400 MeV. When the system reaches thermal equilibrium, the squared adiabatic sped of sound reaches a value close to zero.

5 Conclusions.

Relaxation times obtained via these three signatures show that when the projectile energy is slow, the most important relaxation time is the thermal one, as expected since the available energy is spent in deformation and fragments are emitted from the surface (Fig. 6). But when the projectile energy is high, fragments are emitted from the bulk, and the three relaxation times are the same. Therefore, we expect to obtain low temperatures when the residual is big, since typically this case corresponds to low projectile energies and low excitations. Fig. 7 shows the time evolution for a typical experiment of the central collision Ni+Ni with a low projectile energy equal to 1100 MeV, where as can be seen, the compound suffers deformations up to an asymptotic state and a long quadrupolar relaxation time is expected. In a similar fashion, we expect high temperatures for a high excitation and a high projectile energy, since the relaxation times are short and the system disassembles almost immediately, spending the available energy on heating the system and leading to higher temperatures. When the projectile energy is increased, fragments are no longer emitted from the surface but from the bulk emission, and the dynamical behavior of the system is expected to change, providing different limit temperatures and distinct residual sizes. Work supported by the National Science Foundation (PHY-96-00038), Universidad de Buenos

Aires (EX-070, Grant No. TW98, CONICET Grant No. PIP 4436/96), and Universidad Autónoma Metropolitana-Azcapotzalco (Laboratorio de Cómputo Intensivo).

References

[1] G.F. Bertsch and P.J. Siemens, *Phys. Lett.*B**126**, 9 (1983).

[2] Bao-An Li *et. al.*, *Nucl.Phys.* A **630** 556 (1998).

[3] H. Müller *et. al*,*Phys. Rev.*C**52**, 2072 (1995).

[4] Bao-An Li *et. al*,*Phys. Rev.* C. (2001).

[5] Beaulieu *et. al.*,*Phys.Rev.Lett.* **84** 5971 (2000).

[6] Bao-An Li *et. al.*,*Phys. Rev.* C (1998).

[7] C.M. Hung *et. al*, *Phys. Rev. Lett* **.75**, 4003 (1995).

[8] A. Barrañón *et. al*,*Rev. Mex. Fís.***45**, 110 (1999).

[9] A. Barrañón *et. al.*, *Rev. Mex. Fís.* **47**, 93 (2001). A. Barrañón *et. al..*, *Heavy Ion Phys.* **17**-1, 59 (2003).

[10] A. Strachan and C. O. Dorso, *Phys. Rev.* C**59**, 285(1999).

[11] W. Bauer *et. al.*, *Phys. Rev. Lett.*C**69**, 1888 (1992).

[12] Bao-An Li and S. Yenello, *Phys.Rev.*C**52** 1746 (1995).

[13] A. Strachan and C. O. Dorso, *Phys. Rev.*C**55**, 775(1997).

[14] C. O. Dorso and J. Randrup, *Phys. Lett.*B**301**, 328(1993).

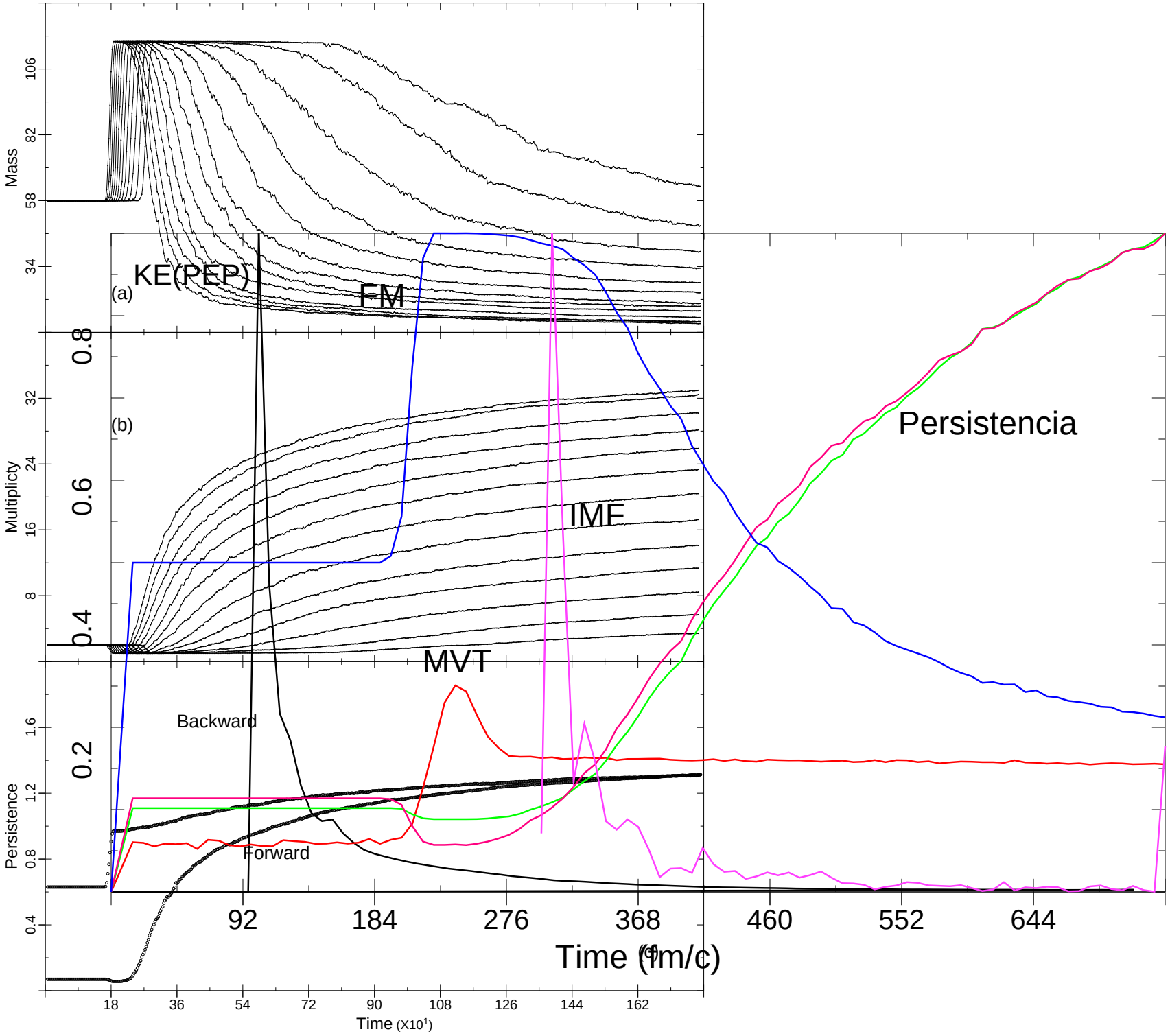
Mass
106
82
58
34
(a)
KE(PEP)
FM
Multiplicty
0.8
0.6
0.4
32
24
16
8
(b)
IMF
MVT
Persistencia
Backward
Forward
Persistence
0.2
1.6
1.2
0.8
0.4
92
184
276
368
460
552
644
Time (fm/c)
18
36
54
72
90
108
126
144
162
Time (X10¹)

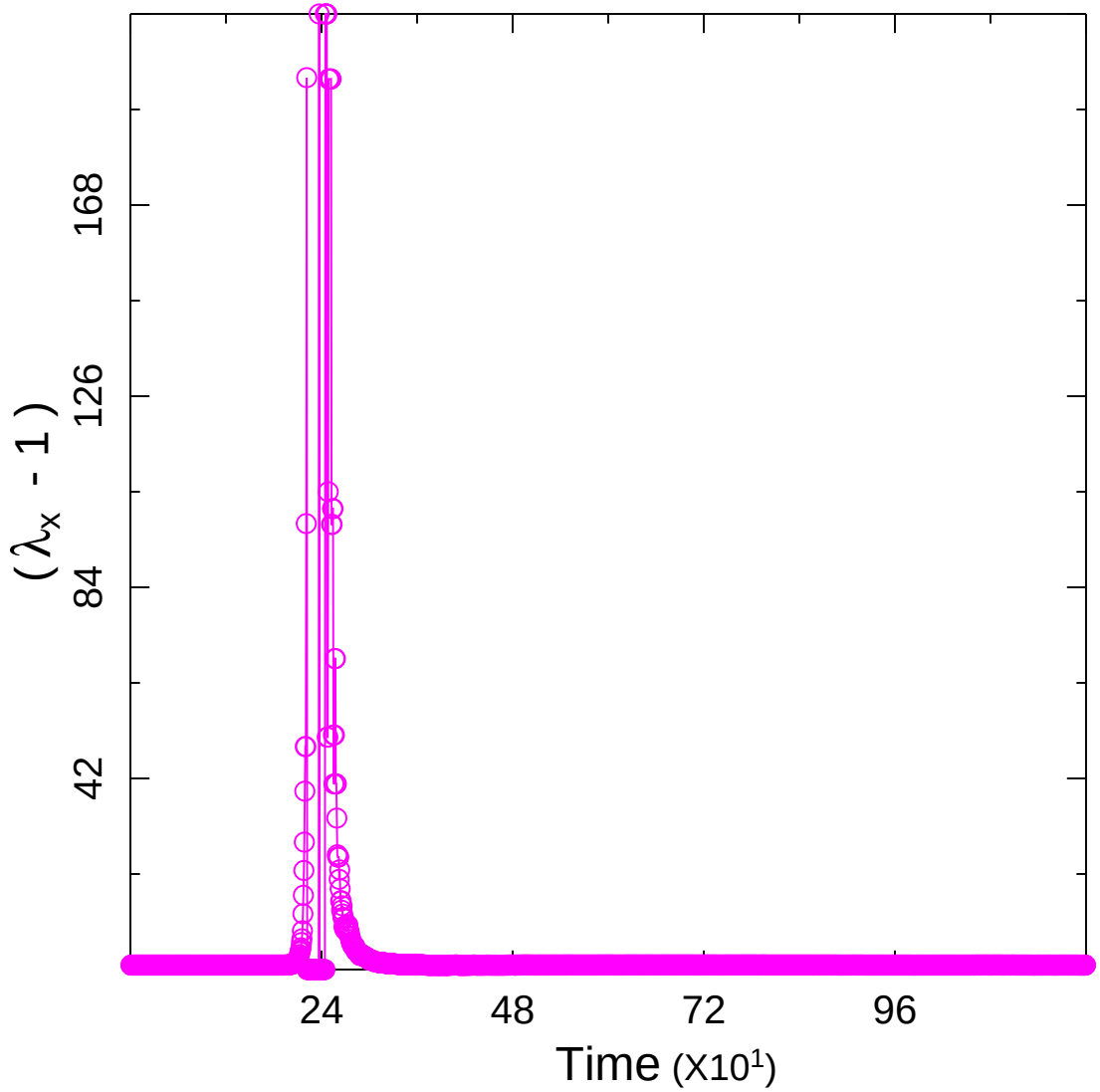
(λ_x - 1)
42
84
126
168
24
48
72
96
Time (X10^1)

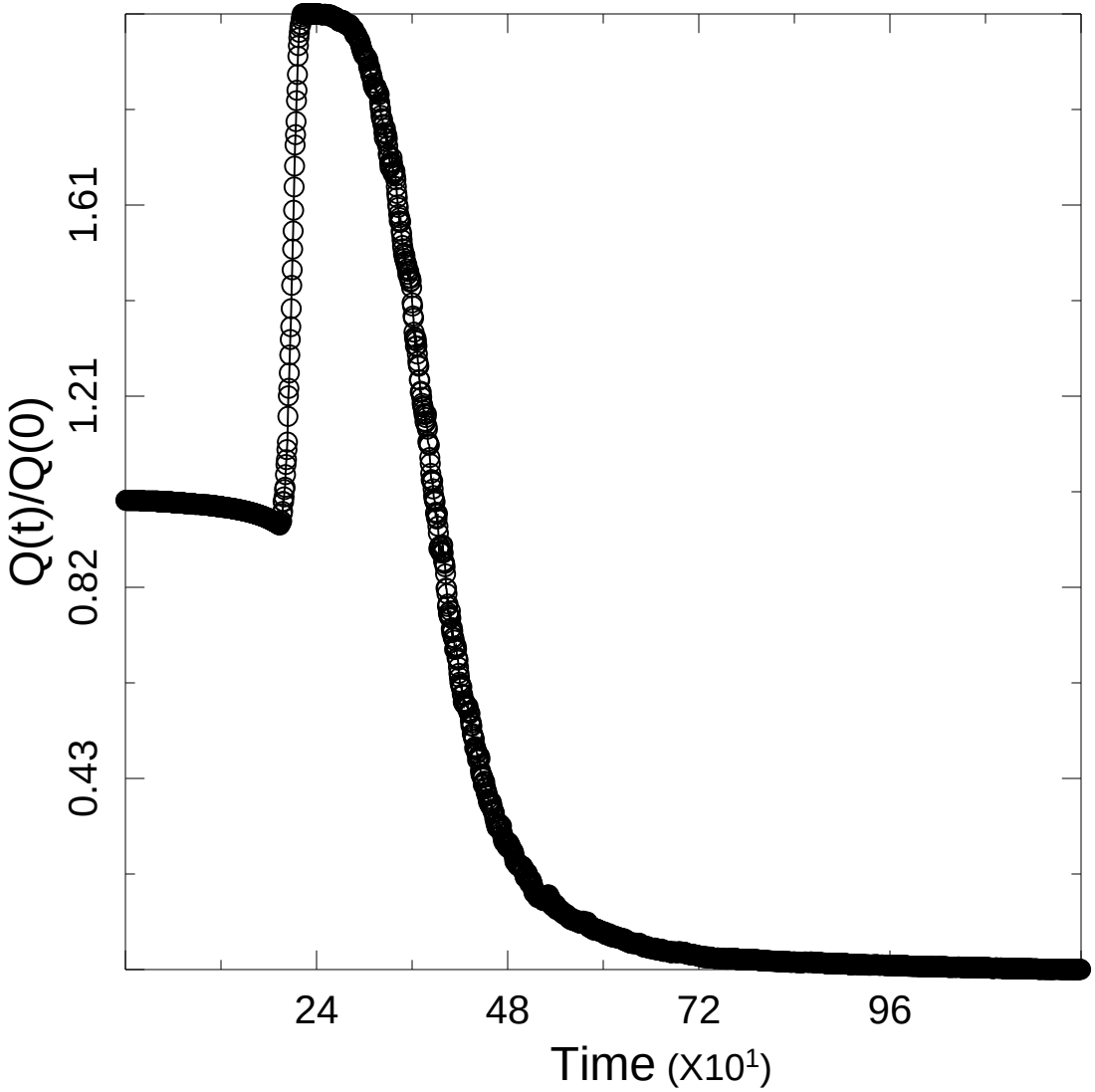
Q(t)/Q(0)
0.43
0.82
1.21
1.61
24
48
72
96
Time (X10[1])

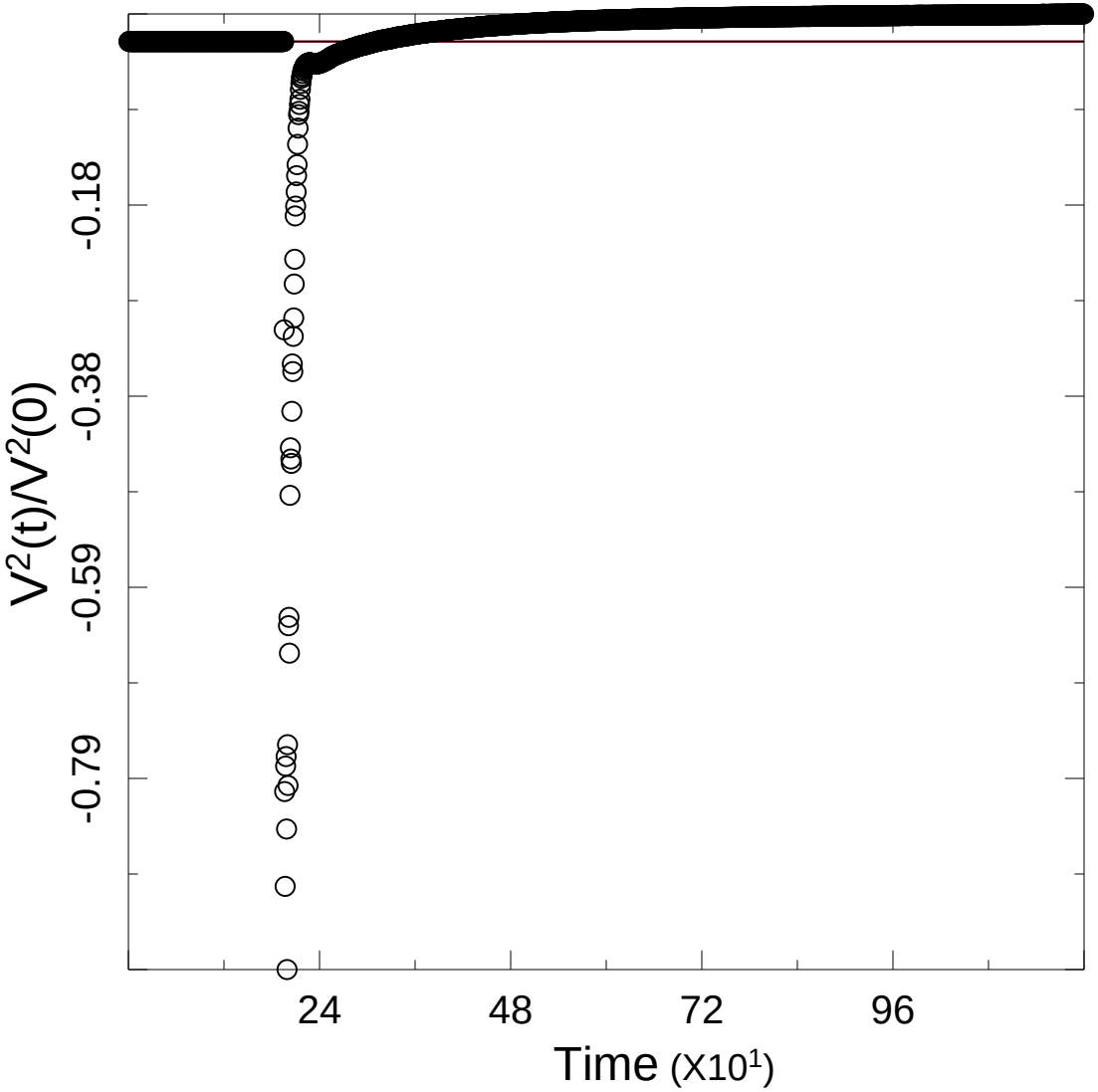
-0.18
-0.38
-0.59
-0.79
V²(t)/V²(0)
24
48
72
96
Time (X10¹)

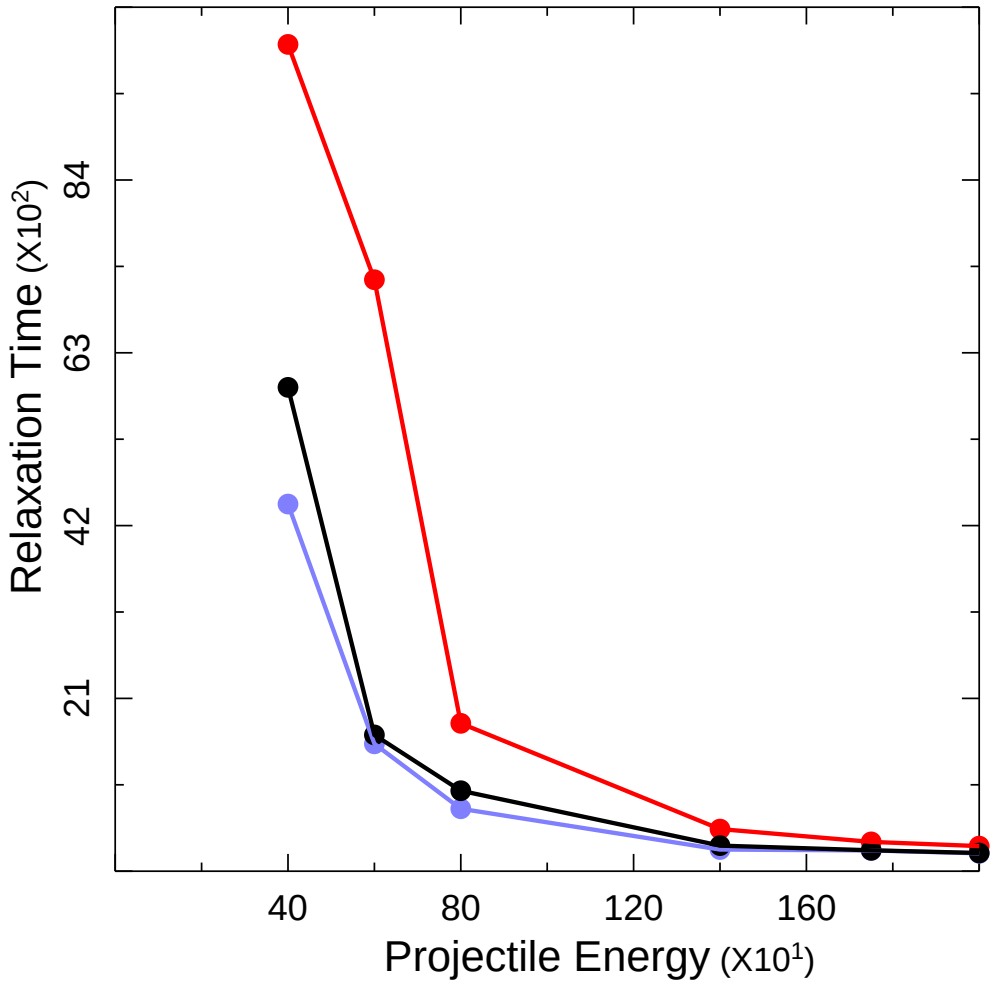
Relaxation Time (X10^2)
84
63
42
21
40
80
120
160
Projectile Energy (X10^1)

This figure "fig7.jpg" is available in "jpg" format from:

http://arXiv.org/ps/nucl-th/0404008v1